Available online at www.sciencedirect.com
ScienceDirect
Journal of Nuclear Materials 373 (2008) 280–288
journal of nuclear materials
www.elsevier.com/locate/jnucmat

# An extension of the two-zone method for evaluating a fission gas release under an irradiation-induced resolution flux

Jin-Sik Cheon *, Yang-Hyun Koo, Byung-Ho Lee, Jae-Yong Oh, Dong-Seong Sohn

*Korea Atomic Energy Research Institute, P.O. Box 105, Yuseong, Daejeon 305-600, Republic of Korea*

Received 19 April 2007; accepted 14 June 2007

**Abstract**

This paper describes an extension of the adaptive two-zone method whose accuracy is substantially enhanced when compared to the original formulation by Matthews and Wood. A diffusive problem under the presence of an irradiation-induced resolution flux is evaluated by applying a variational principle to the diffusion equation. Prior to a gas saturation in the grain boundaries, a constraint associated with a gas balance is added to the variational equation. The spherical grain is divided into two regions whose interface is relocated as the ratio of the number of gas atoms within a grain to that generated. The distribution of the gas concentration is calculated over the grain. During the calculations, the number of degrees of freedoms is reduced to provide a profile which decreases monotonically along the radius. Numerical verifications show that the present approach is viable in computing a gas release accurately and efficiently in fuel performance codes.


*PACS:* 28.41.Ak; 66.30.−h

## 1. Introduction

Fission gas release in a nuclear fuel is modeled by describing a gas transport from a pellet to a free volume. During these complex processes, gas behavior on the grain boundaries plays a key role in determining the diffusive flux from the interior of the pellet [1]. Grain boundary is thermodynamically regarded to behave as a perfect sink to which all the atoms arriving at it are absorbed.

Applying the assumption of a perfect sink to the diffusion problem does not lead to a satisfactory explanation for an incubation observed during a fission gas release. After Speight's argument [2], an irradiation-induced resolution flux has been widely introduced to account for the delay of a gas release. The resolution flux is proportional to the number of gas atoms in the bubbles on a grain boundary. As the gas atoms on a grain boundary reach a certain critical value, the gas atoms are assumed to vent.

A few solutions exist for the gas atoms accumulated on a grain boundary before a saturation [2–4]. In addition, a gas release after a saturation can be evaluated [4,5]. Even with these semi-analytical solutions, it is necessary to obtain their responses through several iterations when time-varying histories are considered. On the other hand there are several numerical solution methods for which the gas concentrations are calculated at nodal points in advance: finite difference method [6], finite element method (FEM) [7,8], and finite volume method [9]. These numerical attempts are more attractive in the sense that they are rather easily extended to versatile situations such as the modification of a boundary condition, time-varying problems, etc. Meanwhile some loss of their accuracy has to be accepted if the number of nodes is not enough and their distribution is not appropriate so that a steep gradient near a grain boundary is not described well and the resolution flux is not computed accurately.

* Corresponding author. Tel.: +82 42 868 2648; fax: +82 42 864 1089.
*E-mail address:* jscheon@kaeri.re.kr (J.-S. Cheon).

0022-3115/$ - see front matter © 2007 Elsevier B.V. All rights reserved.
doi:10.1016/j.jnucmat.2007.06.008

Recently the authors proposed an adaptive two-zone method [10] for which the coordinate of a nodal point changes as a function of the released fraction. This method not only overcomes an inaccuracy at a lower release range, but also it has an efficiency comparable to the Fosberg–Maissh algorithm [11].

In this paper, the adaptive two-zone method is further developed to deal with a fission gas release under an imperfect sink. A system of equations are derived by applying a variational principle to the diffusion equation under a non-homogeneous boundary condition. The gas accumulated at the grain boundaries and its release to the free volume are computed from the profile of the gas concentration. It is also of importance to compare these results with those from previous analytic solutions and the FEM.

## 2. Fission gas release under irradiation-induced resolution condition

The diffusion equation in spherical coordinates,

$$\frac{\partial c_g}{\partial t} = \frac{1}{r^2}\frac{\partial}{\partial r}\left(Dr^2\frac{\partial c_g}{\partial r}\right) + \beta, \tag{1}$$

is solved with the boundary conditions, $c_g = c_\lambda$ at $r = a$ and $\partial c_g/\partial r = 0$ at $r = 0$, where $a$ is the grain radius, $D$ the effective diffusion coefficient of a gas atom, and $\beta$ the gas atom generation rate. The values $c_\lambda$ and $\beta$ are defined depending on how the irradiation-induced resolution flux near a grain boundary is taken into account.

Following Speight's argument [2], although there is controversial discussion on its validity [12], the diffusive flux within the matrix to the boundary is assumed to be balanced by the resolution flux from the boundary, i.e.

$$\frac{Dc_\lambda}{\lambda} = \frac{bN}{2}, \tag{2}$$

where $b$ is the rate of a resolution of the intergranular atoms, $N$ the gas atoms per unit area of a grain face, $\lambda$ the thickness of a resolution layer, and $c_\lambda$ the average gas concentration in the resolution layer.

When the perfect sink boundary condition is preserved, all the atoms due to a resolution provide an additional flux at a depth of $\lambda$, or an additional source term which is distributed uniformly throughout a layer [6]. In combination with the perfect sink boundary condition, the solutions are obtained by adding the resolution flux to the source term. On the other hand, the diffusion equation under the resolution flux is also solved by adopting an imperfect boundary condition [4,5,9]. Rearranging Eq. (2) yields the boundary condition

$$c_\lambda = \frac{\lambda bN}{2D}. \tag{3}$$

As the gas is accumulated on a grain face via a resolution, $N$ is saturated at a value of $N_{sat}$. The saturation concentration is fixed for all the temperatures [13].

During the computations, $N$ is evaluated from a balance among the gas atoms generated, those remaining within a grain, those in a grain boundary, and those released:

$$\int \beta \mathrm{d}t = \bar{c}_g + 3N/2a + R, \tag{4}$$

where $\bar{c}_g$ is the average gas concentration in the grain, and $R$ is the number of gas atoms released per unit volume of a fuel.

After a saturation, all the gas arriving at a grain boundary is released. Gas released fraction to the free volume is determined by

$$f = 1 - \frac{\bar{c}_g + 3N_{sat}/2a}{\int \beta \mathrm{d}t}. \tag{5}$$

### 2.1. Steady-state condition

Speight [2] suggested an approximate method for the rate of an accumulation of gas atoms at a grain face. It is given by

$$\frac{\mathrm{d}N}{\mathrm{d}t} = 4\beta\left(\frac{Dt}{\pi}\right)^{1/2}\left(1 - \frac{Nb\lambda}{2D\beta t}\right). \tag{6}$$

The solution [6] for Eq. (6) is written in the form of

$$N = A'(u^2 - 2u + 2 - 2\exp(-u)), \tag{7}$$

where $A' = \beta\pi D^2/8(b\lambda)^3$ and $u = 4b\lambda(t/D\pi)^{1/2}$.

Gas release after the saturation of a grain boundary was obtained by Turnbull [5], based on the assumption of a uniform gas concentration within a grain. It was evaluated that the fractional release shows an overestimation after an incubation when a variation of the gas concentration across the grain is pronounced under certain conditions such as a high temperature, and a low resolution rate [6]. Thus the following numerical methods are desirable to seek a reference solution.

### 2.2. Time-varying condition

Nuclear fuels are normally irradiated under varying power conditions. Even when a pin power remains constant, the fuel temperature varies with time due to a change in the gap conductance, a reduction of the thermal conductivity of a pellet, etc. Therefore a suitable algorithm is required to obtain a gas accumulation on a grain boundary and a fission gas release after a saturation under varying temperature conditions.

A few iterations are inevitable to develop a transient solution for all the algorithms which have been developed up to now. Based on the Booth [14] solutions, a composite release equation proposed by Turnbull [15] provides the fractional release by solving an effective time iteratively. Also an integro-differential equation for the gas accumulated on a grain face and the gas release were rigorously derived by Forsberg and Massih [4]. However, it still needs to be treated numerically for time-varying conditions.

As for purely numerical methods [6,7,9], the gas concentrations at nodal points are calculated in advance. The gas accumulation on a grain boundary and the fractional release are obtained by integrating the profile of a gas concentration. As stated above, the diffusion equation can be numerically solved by incorporating the resolution flux together with a perfect sink boundary condition or under a non-homogeneous boundary condition to account for a resolution. Regardless of the approaches, the numerical treatment to obtain gas concentrations at nodal points leads to a set of simultaneous equations:

$$\mathbf{K}\mathbf{c}_g = \mathbf{b}, \tag{8}$$

where $\mathbf{K}$ represents the global stiffness matrix, $\mathbf{c}_g$ the concentration vector, and $\mathbf{b}$ the load vector. As $N$ depends on $\mathbf{c}_g$ before a grain-face saturation, a few iterations are required until the mass balance of Eq. (4) is satisfied.

### 2.3. Reference solution from the finite element method

We employed the FEM to prepare the reference solutions for $N$ and $f$ where $\bar{c}_g$ is required as given by Eqs. (4) and (5), respectively. The diffusion equation with a non-homogeneous boundary condition is solved by modifying a system of equations, resulting from eliminating $c_\lambda$ from the independent variables.

At every moment, $\bar{c}_g$ is evaluated with the gas concentrations at the nodal points as follows:

$$\bar{c}_g = \sum_{i=1}^{n} k_i c_i, \tag{9}$$

where $n$ is the number of nodal points, $c_i$ is the element of $\mathbf{c}_g$, and $k_i$ is the coefficient for $c_i$. $c_n$ corresponds to $c_\lambda$. The expression for $k_i$ is not only determined by the coordinate of the nodal points, but also is dependent on which numerical method is chosen to obtain $\mathbf{c}_g$.

By inserting Eq. (9) and (4) into Eq. (3), and eliminating $N$, $c_\lambda$ is represented by

$$c_\lambda = \frac{\Lambda\left(G - R - \sum_{i=1}^{n-1} k_i c_i\right)}{1 + \Lambda k_n}, \tag{10}$$

where $\Lambda = \lambda ba/3D$ and $G = \int \beta \mathrm{d}t$.

Thus the gas concentration at the boundary is a function of the gas concentrations at the remaining nodal points. The linear dependency of $c_\lambda$ on $c_i$ exhibited in Eq. (10) is introduced by applying a multi-point (multi-freedom) constraint (MPC) to the problem. There are several methods to treat an MPC such as a master–slave elimination, a penalty, Lagrange multiplier, etc.

For reference solutions, the number of finite elements (FE) is 50 to represent a grain. The grain is divided into two layers whose interface is located at an order of a magnitude of $\lambda$ from the grain surface. The inner and outer layers have 40 and 10 quadratic elements, respectively. The ratio of the element length is 1.1 and 1.0 for the two layers. The number of FE and the distribution of the nodal points are the same as those utilized in the previous works [6,10].

Imposing an MPC in Eq. (8) is done by the master–slave elimination method [16], which changes $\mathbf{K}$ and $\mathbf{b}$ to produce a modified system of the equations. This procedure causes the present problem to be linear, at least, if the parameters including $N_{sat}$ do not vary with time. After a saturation, the condition of an MPC is removed and the gas release commences.

## 3. Adaptive two-zone method under an imperfect boundary condition

The adaptive two-zone method [10] follows a similar approach adopted by Matthews and Wood [17]. The variational principle is applied to calculate a fission gas release from a spherical grain which is divided into two regions. The accuracy of the original two-zone approximation, however, is substantially improved by implementing two strategies. Firstly the interface of the two regions is moved in proportion to the released fraction. Secondly the number of degree of freedoms (DOF) is reduced to provide a physically admissible profile of a gas concentration which decreases monotonically from the center to the surface. We extended this formulation to the imperfect sink condition.

### 3.1. Trial functions

The two regions are designated as region I and II, respectively. Three nodal points are required; the midpoint radius of region I ($\rho_1 = 0.4$), the midpoint radius of region II ($\rho_3 = 0.9$), and the interface between the two regions, $\rho_2$. The normalized radius, $\rho$ is defined by $r/a$. For the perfect sink boundary condition [10], the interface $\rho_2$ is updated by a linear equation as follows:

$$\rho_2(t) = 1 - \kappa_d \cdot f_u(t), \tag{11}$$

where $\kappa_d$ is a factor controlling the update of $\rho_2$, and $f_u$ is $1 - \bar{c}_g/G$. The lower limit of $\rho_2$ is 0.8. We assumed that the same relations of $\rho_2(t)$ and $f_u$ are applicable for an imperfect sink problem. $\kappa_d$ is chosen to be 0.5 in our calculations.

The concentrations at $\rho_1$, $\rho_2$, and $\rho_3$ are represented by $c_1$, $c_2$, and $c_3$, respectively. In the case of the imperfect sink problem, the gas concentration at the grain face, $c_0$ is necessary since it varies with time as given by Eq. (3). The concentration profile in each region is described by the quadratic trial functions, $C_1$ and $C_2$ which are a function of $\rho_2$.

$C_1$ and $C_2$ are derived by applying the boundary condition, $\partial c_g/\partial r = 0$ at $\rho = 0$, $c_g = c_0$ at $\rho = 1$, and a continuity of the gas concentration at $\rho_2$. The trial functions are as follows:

For the inner region,

$$C_1(\rho) = \frac{25\left(\rho_2^2 - \rho^2\right)}{25\rho_2^2 - 4} c_1 + \frac{25\rho^2 - 4}{25\rho_2^2 - 4} c_2, \tag{12}$$

and for the outer region,

$$C_2(\rho) = \frac{(\rho-1)(2\rho-\rho_2-1)}{(\rho_2-1)^2}c_2 + \frac{4(\rho-1)(\rho_2-\rho)}{(\rho_2-1)^2}c_3 + \frac{(\rho_2-2\rho+1)(\rho_2-\rho)}{(\rho_2-1)^2}c_0. \quad (13)$$

### 3.2. Stiffness matrix and load vector

The gas concentration $c_g^0$ at a time $t$ becomes $c_g$ after an increment of time $\delta t$. After integrating the diffusion equation for $\delta t$ by using the backward Euler method, the variational form is derived by taking the product of the time-integrated diffusion equation with a trial function and integrating it over the domain.

In a comparison with our previous work [10], we added a constraint to the variational equation before a gas saturation on a grain face. The constraint is

$$c_0 = \Lambda\left(G - R - \bar{c}_g\right), \quad (14)$$

where $\bar{c}_g = k_1c_1 + k_2c_2 + k_3c_3 + k_0c_0$. The coefficients of $\bar{c}_g$ are dependent on $\rho_2$, and are defined below.

The Lagrange multiplier method adds a constraint to the original variational equation, yielding

$$\delta\int_0^a 4\pi\left[\frac{D_{\text{eff}}}{2}\left(\frac{\mathrm{d}c_g}{\mathrm{d}r}\right)^2 + \frac{c_g^2}{2\delta t} - \left(\frac{c_g^0}{\delta t}+\beta\right)c_g\right]r^2\mathrm{d}r + \delta\lambda_c 4\pi a^3\left[c_0 - \Lambda\left(G-R-\bar{c}_g\right)\right] = 0, \quad (15)$$

where $\lambda_c$ is the Lagrange multiplier.

Inserting the trial functions into Eq. (15) and minimizing the integral with respect to $c_1$, $c_2$, $c_3$, $c_0$, and $\lambda_c$ leads to a set of equations as Eq. (8). Some of the elements of **K** and **b** are a function of $\rho_2$.

Non-zero elements of the symmetric matrix **K** are given by

$$\begin{aligned}
K_{11} &= \frac{50A_8}{W_1^2}\frac{D_{\text{eff}}}{a^2} + \frac{10A_8A_9}{21W_1^2}\frac{1}{\delta t},\\
K_{12} &= -\frac{50A_8}{W_1^2}\frac{D_{\text{eff}}}{a^2} + \frac{A_1A_8}{21W_1^2}\frac{1}{\delta t},\\
K_{22} &= \frac{A_2}{15W_1^2W_2}\frac{D_{\text{eff}}}{a^2} + \frac{A_3}{210W_1^2}\frac{1}{\delta t},\\
K_{23} &= -\frac{2A_4}{15W_2}\frac{D_{\text{eff}}}{a^2} + \frac{A_5W_2}{105}\frac{1}{\delta t},\\
K_{33} &= \frac{16A_6}{15W_2}\frac{D_{\text{eff}}}{a^2} + \frac{8A_7W_2}{105}\frac{1}{\delta t},\\
K_{24} &= \frac{A_{10}}{15W_2}\frac{D_{\text{eff}}}{a^2} - \frac{A_{11}W_2}{420}\frac{1}{\delta t},\\
K_{34} &= -\frac{2A_{12}}{15W_2}\frac{D_{\text{eff}}}{a^2} - \frac{A_{13}W_2}{105}\frac{1}{\delta t},\\
K_{44} &= \frac{A_{14}}{15W_2}\frac{D_{\text{eff}}}{a^2} + \frac{A_{15}W_2}{210}\frac{1}{\delta t},
\end{aligned} \quad (16)$$

where $W_i$s and $A_i$s are defined in Appendix A. In addition, four non-zero elements are needed due to an introduction of the Lagrange multiplier,

$$\begin{aligned}
K_{51} &= \Lambda k_1,\\
K_{52} &= \Lambda k_2,\\
K_{53} &= \Lambda k_3,\\
K_{54} &= (1+\Lambda k_0).
\end{aligned} \quad (17)$$

By virtue of a small difference of $\rho_2$ relative to $\rho_{20}$, $\rho_2$ at a previous time increment [10], **b** is simply approximated by

$$b_i \approx \left(\hat{b}_{i,0} + \hat{b}_{i,1}(\rho_{20}-\rho_2)\right)\Big/\check{b}_i, \quad (18)$$

where $\check{b}_i$ and $\hat{b}_{i,j}$ are the denominator and the coefficient of the numerator, respectively. $\hat{b}_{i,0}$ and $\hat{b}_{i,1}$ are summarized in Table 1, and the $Y_i$s are given in Appendix A. $\check{b}_i$s are given by

$$\begin{aligned}
\check{b}_1 &= 21\delta t\, W_1W_{10}/A_8,\\
\check{b}_2 &= 420\delta t\, W_1W_{10},\\
\check{b}_3 &= 105\delta t\, W_{10},\\
\check{b}_4 &= 420\delta t\, W_{10}.
\end{aligned} \quad (19)$$

The last element of **b** is of the form

$$b_5 = G\Lambda. \quad (20)$$

Since $c_0$ is constrained with the rest of the elements of $\mathbf{c}_g$ through Eq. (14), $c_1$, $c_2$, and $c_3$ are independent except for $\lambda_c$.

Similarly the stiffness matrix and the load vector after a gas saturation are derived by using the boundary condition, $c_0 = c_{\text{sat}}$. Non-zero elements of **K** are the same as $K_{11}$, $K_{12}$, $K_{22}$, $K_{23}$, and $K_{33}$ in Eq. (16). Elements of the load vector, $b_i^{\text{sat}}$ are obtained by modifying the three elements of **b** as given by

$$\begin{aligned}
b_1^{\text{sat}} &= b_1,\\
b_2^{\text{sat}} &= b_2 - c_{\text{sat}}K_{24},\\
b_3^{\text{sat}} &= b_3 - c_{\text{sat}}K_{34},
\end{aligned} \quad (21)$$

where $b_i$ is the element of **b** in Eq. (18).

The coefficients of $\bar{c}_g$ are derived as $k_1 = A_8/W_1$, $k_2 = Y_1/20W_1$, $k_3 = W_2Y_6/5$, and $k_0 = -W_2Y_{11}/20$.

### 3.3. Solutions of the system

The system of equations can be solved easily. However spurious fluctuations along the grain radius could occur if all the DOFs are used during the whole stage of a calculation [10]. We can cause the gas concentration to decrease monotonically by reducing the number of DOFs of the system. The number of DOFs is decreased by imposing a homogeneous constraint on the system of equations. The master–slave elimination method is employed to deal with the constraint. A new set of DOFs $\hat{\mathbf{b}}$ is prepared by removing all the slave freedoms from **b**. A matrix transformation is used to relate $\hat{\mathbf{b}}$ to **b**

Table 1
Coefficients of the numerators of the load vector

| | $\hat{b}_{i,j} = \zeta \cdot \beta\delta t + \xi_1 \cdot c_{10} + \xi_2 \cdot c_{20} + \xi_3 \cdot c_{30} + \xi_0 \cdot c_{00}$ | | | | |
|---|---|---|---|---|---|
| | $\zeta$ | $\xi_1$ | $\xi_2$ | $\xi_3$ | $\xi_0$ |
| $\hat{b}_{1,0}$ | $7W_1$ | $10A_9$ | $A_1$ | 0 | 0 |
| $\hat{b}_{1,1}$ | $Y_8$ | $Y_8$ | 0 | 0 | 0 |
| $\hat{b}_{2,0}$ | $7W_1Y_1$ | $20A_1A_8$ | $2A_3$ | $4A_5W_1^2W_2$ | $-A_{11}W_1^2W_2$ |
| $\hat{b}_{2,1}$ | $Y_1Y_8$ | $70A_9^2Y_7$ | $2W_1Y_2$ | $-8W_1Y_3$ | $2W_1Y_9$ |
| $\hat{b}_{3,0}$ | $7W_1W_2Y_6$ | 0 | $A_5W_1W_2$ | $8A_7W_1W_2$ | $-A_{13}W_1W_2$ |
| $\hat{b}_{3,1}$ | $W_2Y_6Y_8$ | 0 | $Y_4$ | $-4Y_5$ | $-Y_{10}$ |
| $\hat{b}_{4,0}$ | $-7W_1W_2Y_{11}$ | 0 | $-A_{11}W_1W_2$ | $-4A_{13}W_1W_2$ | $2A_{15}W_1W_2$ |
| $\hat{b}_{4,1}$ | $-W_2Y_8Y_{11}$ | 0 | $-Y_{12}$ | $4Y_{13}$ | $-Y_{14}$ |

$$\mathbf{b} = \mathbf{T}\hat{\mathbf{b}}. \tag{22}$$

A new system of equations is obtained by modifying Eq. (8) as follows:

$$\widehat{\mathbf{K}}\hat{\mathbf{c}}_g = \hat{\mathbf{b}}, \tag{23}$$

where $\widehat{\mathbf{K}} = \mathbf{T}^T\mathbf{K}\mathbf{T}$, and $\hat{\mathbf{c}}_g = \mathbf{T}^T\mathbf{c}_g$.

Before the grain-face saturation, the profile of the gas concentration within a grain is obtained by solving the system of equations. If the gas concentration does not decrease monotonically along the radius, $c_1$ is set to be equal to $c_2$. In addition we eliminate $c_3$ from the DOFs by introducing a constraint $\partial C_2/\partial\rho = 0$ at $\rho_2$. This leads to $c_3 = 3c_2/4 + c_0/4$. The matrix form of the transformation (22) is

$$\begin{pmatrix} c_1 \\ c_2 \\ c_3 \\ c_0 \\ \lambda_c \end{pmatrix} = \begin{pmatrix} 1 & 0 & 0 \\ 1 & 0 & 0 \\ \frac{3}{4} & \frac{1}{4} & 0 \\ 0 & 1 & 0 \\ 0 & 0 & 1 \end{pmatrix} \begin{pmatrix} c_2 \\ c_0 \\ \lambda_c \end{pmatrix}. \tag{24}$$

Furthermore, if the modified system provides a solution such that $c_2$ is less than $c_0$, we eliminate $c_0$ from the DOFs by adding a constraint $c_0 = c_2$. The matrix form of the transformation (22) is

$$\begin{pmatrix} c_1 \\ c_2 \\ c_3 \\ c_0 \\ \lambda_c \end{pmatrix} = \begin{pmatrix} 1 & 0 \\ 1 & 0 \\ 1 & 0 \\ 1 & 0 \\ 0 & 1 \end{pmatrix} \begin{pmatrix} c_2 \\ \lambda_c \end{pmatrix}. \tag{25}$$

When the reduced system of Eq. (23) is solved, all the solutions are recovered.

After a grain-face saturation, one may refer to the solution procedure reported in our previous work [10]. It is observed that the system of equations has a matrix structure identical to that in the perfect sink case. Thus the solution is one of the forms as derived for the cases with 1-DOF, 2-DOFs, and 3-DOFs. The number of DOFs is selected to guarantee that the profile of the gas concentration decreases along the radius. A reduced system of equations could be obtained by applying a matrix transformation of Eq. (22) to the system of equations as explained above for the solution procedure before a grain-face saturation. Meanwhile the apex of $C_2$, $\rho_{2v}$ needs to be redefined

$$\rho_{2v} = \frac{c_2(3+\rho_2) - 4c_3(1+\rho_2) + c_0(1+3\rho_2)}{4(c_2 - 2c_3 + c_0)}. \tag{26}$$

We employed the same procedures as those reported in [10] for the convergence criterion as well as the automatic time integration. Prior to a grain-face saturation, the number of gas atoms on a grain face is chosen to determine a convergence and a time increment. After a saturation, these are checked by means of the released fraction. At every time step, several iterations are required to satisfy the convergence criterion.

In a reference problem with an irradiation-induced resolution flux, the computational time of the adaptive two-zone method is comparable to that of the case with a perfect sink boundary condition.

## 4. Verification of the adaptive two-zone method under an imperfect boundary condition

The validity of the proposed method is examined by comparing its responses with the reference solutions for a number of temperature and gas generation conditions. The fission rate is assumed to be linearly proportional to the temperature. To confirm the soundness of the present method as a numerical algorithm, an FEM solution with 50 quadratic elements is obtained for every calculation.

The expression for the diffusion coefficient of the gas atoms is given in Ref. [6]. A grain radius of 5 μm and a thickness of the resolution layer of 0.01 μm are used in the calculations. It is assumed that the number of gas atoms on a grain face is saturated at a value of $2 \times 10^{19}$ atoms/m$^2$. The resolution rate is linearly proportional to the fission density, and the reference fission density is taken at a linear power of 20 kW/m.

Prior to the verifications of the present method, the applicability of the imperfect boundary condition of Eq. (3) is examined by comparing its fractional saturations with those from an FEM.

Fig. 1 shows the number of gas atoms accumulated on a grain boundary as a function of the normalized time for a

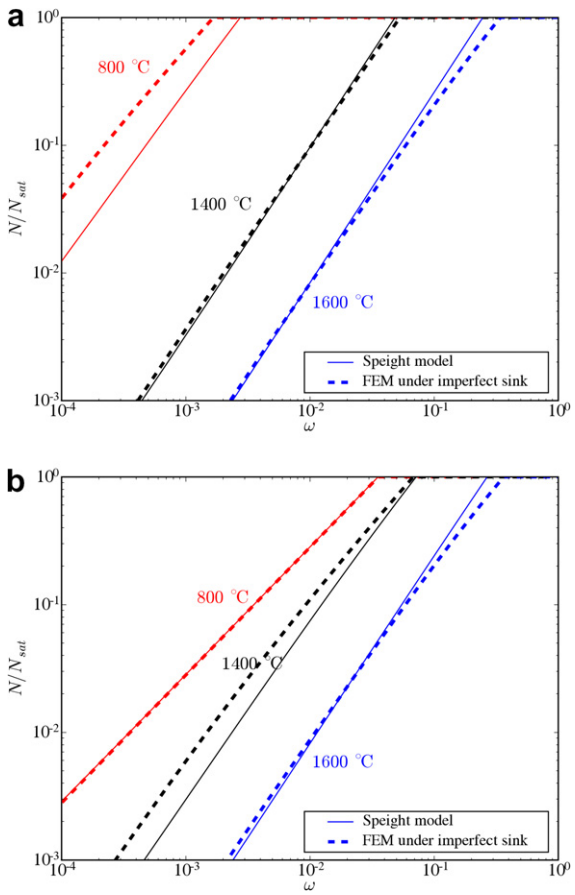


Fig. 1. Comparison of the gas saturation behaviors between Speight model and FEM calculation with 50 elements. (a) $b = 10^{-6}$, (b) $b = 3 \times 10^{-5}$.

series of constant temperatures. Speight's solution given by Eq. (7) is plotted by a solid line, and the response from the FEM by a dotted line. It is observed that, in a comparison with the Speight's model, the FE solutions provide an earlier saturation at low temperatures. This situation results from the imperfect sink boundary condition of Eq. (3) for which the gas concentration at a grain surface is assumed to be already equal to the value at a depth of a resolution layer. The difference is especially pronounced in Fig. 1(a) where the resolution rate is small ($b = 10^{-6}\ s^{-1}$) and the temperature is at a value of 800 °C. Under such conditions, the response of a saturation at a grain boundary follows the dependency of $t^{3/2}$ which is obtained by decreasing $u$ in Eq. (7). However the normalized time is too low to cause the incubation times to be practically different between the two results. At the temperature of 1600 °C, on the other hand, the FE response lies behind the Speight's solution which is not applicable because a short-term ($Dt/a^2 \ll 1$) approximation of the Booth [14] solution is employed.

The comparisons for $b = 3 \times 10^{-5}\ s^{-1}$ are presented in Fig. 1(b). The saturation curves at 800 °C become indiscernible when the diffusive flux is overwhelmed by the resolution flux due to an increase of the resolution rate. Instead the difference between the two results is calculated to appear at a higher temperature. At 1400 °C, the gas atoms are shown to be accumulated earlier on a grain boundary for the imperfect sink model. It is interpreted that the additional resolution flux from a grain boundary due to an increase of the resolution rate is competing with an enhanced diffusive flux from the interior of a grain at a higher temperature. Meanwhile, the discrepancy is reduced to a negligible magnitude at the occurrence of a saturation.

As the temperature is further raised, the response of the gas saturation is almost the same irrespective of the value of $b$. It is thought that, under a higher temperature, the gas concentration at a grain boundary as given by Eq. (3) is dominated mainly by the diffusion process.

Fig. 2 shows the calculated results for the gas atoms at a grain boundary, and the fractional gas release as a function of the normalized time for $b = 5 \times 10^{-5}\ s^{-1}$. It appears that the discrepancies in the saturation behaviors are negligible between the reference FEM and the present method. Even at a high temperature the adaptive two-zone method predicts incubation behaviors which are similar to the FEM results. As for the fractional release, the results from the present method coincide well with those from the FEM. At a temperature of 800 °C, there is a minor difference in the fractional release between the two methods, which can be considered to be acceptable.

Fig. 3 is the saturation behavior as a function of the irradiation time when the temperature is subjected to changes. Fractional saturation curves are shown to follow a similar tendency. At the moment of a stepwise change of the temperature, however, the fractional saturation drops abruptly for the present calculation while it varies continuously for the FEM.

Fig. 4 shows the dependencies of the fractional gas release on the irradiation time. Two curves are in excellent agreement during a power increase as well as a power decrease.

The adaptive two-zone method has been extensively verified by applying the methodology proposed by Lassmann

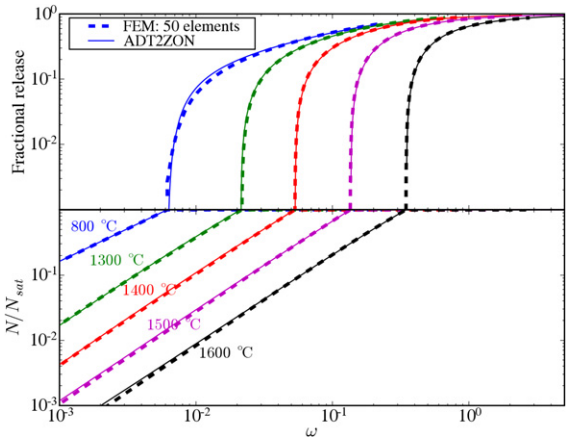


Fig. 2. Calculated fractional gas saturation and fractional gas release as a function of the time under $b = 5 \times 10^{-6}$ at various temperatures. The present method is represented by ADT2ZON.

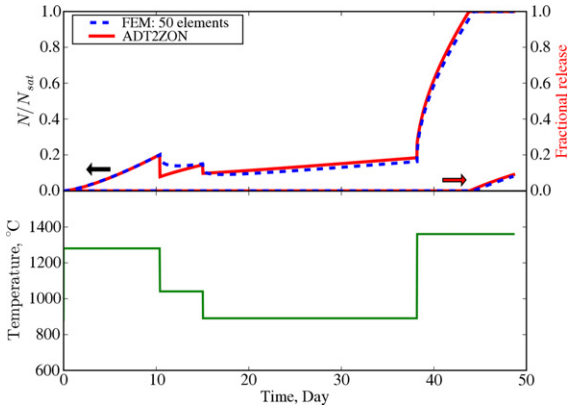


Fig. 3. Calculated fractional saturation as a function of the time for varying gas generation under $b = 3 \times 10^{-6}$.

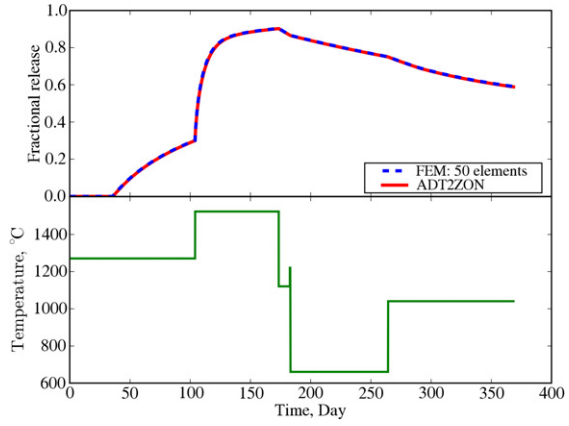


Fig. 4. Calculated fractional release as a function of the time for varying gas generation under $b = 3 \times 10^{-6}$.

and Benk [18]. The fractional gas releases are calculated for a set of 2000 individual power histories which is the same as those used for a verification of the problem with a perfect sink assumption at a grain boundary [10]. The results are compared with the reference FEM solutions in Fig. 5. The number of cases in which a gas release is absent is 1293 for both the present method and the FEM. After a release of fission gas, the adaptive two-zone method shows a good overall behavior. In view of the fact that the present results are obtained by employing 1–4 nodes in comparison with the 101 nodes for the FEM, this comparison proves the superior capability of the present approach for a broad range of fission gas release.

The validity of the adaptive two-zone method is further confirmed by plotting the fractional releases under an imperfect sink with respect to those under a perfect sink. A comparison is presented in Fig. 6. As expected, the fractional release is retarded under the circumstances with an irradiation-induced resolution flux. There exists no exceptional case for such a trend.

The distribution of the number of verification cases against the fractional release is shown in Fig. 7. In the case

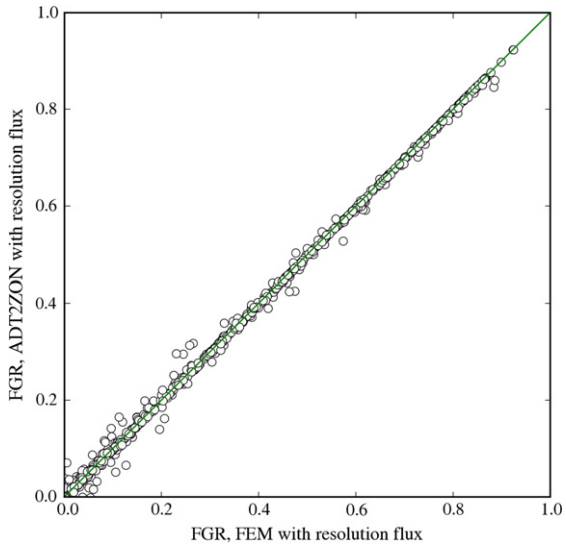


Fig. 5. Present method versus FEM with 50 elements under $b = 3 \times 10^{-6}$.

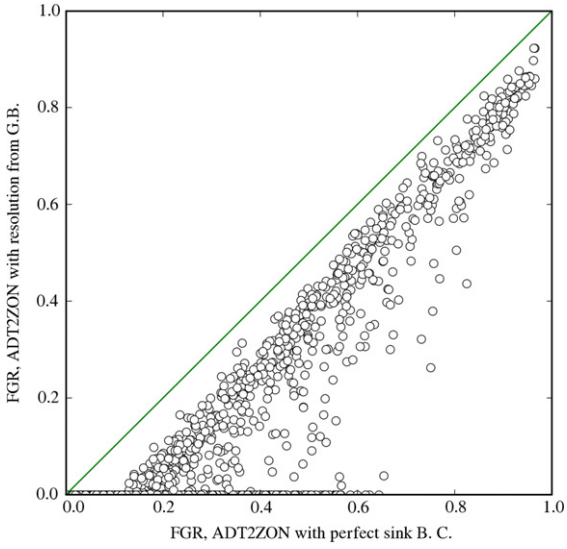


Fig. 6. Comparison between fractional releases with irradiation-induced resolution from grain boundary ($b = 3 \times 10^{-6}$) and those under perfect sink boundary condition.

of a perfect sink condition, the number of cases follows a normal distribution with a mean of zero, which is obtained by using the ANS-5.4 algorithm [10,19]. Imposing an imperfect sink on a grain boundary results in suppressing the fission gas release especially in a low range of less than 0.4. There is a good agreement between the current approach and the FEM.

## 5. Discussion

The above results show that the adaptive two-zone method predicts fission gas behaviors comparable to the FEM with fine meshes. However, the present method causes an abrupt drop in the fractional saturation as shown

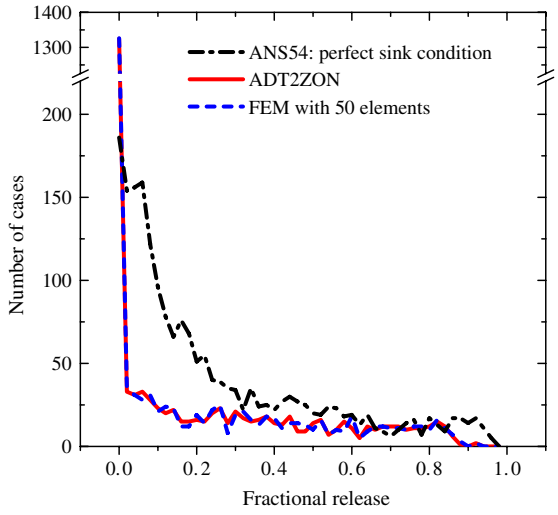


Fig. 7. Distribution of the number of cases with respect to fractional release under $b = 3 \times 10^{-6}$.

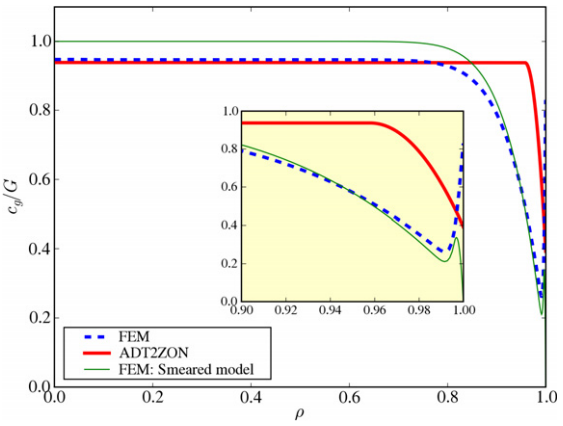


Fig. 8. Normalized gas concentrations along normalized radius at the time of 10.5 days under $b = 3 \times 10^{-6}$.

in Fig. 3. Under the temperature history of Fig. 3 the distribution of a gas concentration was investigated.

Fig. 8 is the profile of a gas concentration in a grain at the time of 10.5 days. Even though a gas accumulation is not seen within a depth of a resolution layer for the current approach, it is unlikely that such a sudden drop in the fractional saturation is accomplished by promptly redistributing a resolution flux over a whole grain. In comparison, it is shown that there is a reverse gradient of the gas concentration near a surface for the case of an FEM. A similar accumulation near the surface is also manifested in the case that an FE calculation is performed by implementing an effective generation rate to a resolution layer under a perfect sink. These tendencies are more pronounced when a larger amount of the power level is decreased at a power transition. In this way there could appear an unfavorable situation where a gas concentration on the surface exceeds the number of gas atoms generated by the fission per unit volume, since the gas atoms accumulated do not diffuse away due to a lower temperature.

In addition to these observations, the assumption of Eq. (2) is nullified for the calculation of a fission gas release at a higher temperature as discussed by White [12]. Speight [2] introduced the assumption in order to resolve the phenomenon that most of fission gas atoms are released in 2 to 3 days at 1400 °C. As shown in Fig. 1, however, the resolution flux prevails by the diffusion flux at a temperature higher than 1400 °C.

As a result, it is necessary that further studies should be devoted to better understanding an incubation behavior in relation with the validity of an irradiation-induced resolution boundary condition.

## 6. Conclusion

An adaptive variational method has been derived to solve the diffusion equation for a fission gas release with an irradiation-induced resolution on a grain boundary. Extensive verifications have shown the effectiveness and accuracy of this approach to predict the incubation behavior of a gas release as well as a fractional release. In a similar way it could be further extended in an attempt where one needs to develop a more descriptive model by incorporating auxiliary equations to represent a gas flow from a grain boundary to a free volume.

## Acknowledgement

The Ministry of Science and Technology (MOST) of the Republic of Korea has sponsored this work through the Mid- and Long-term nuclear R&D Project.

## Appendix A

The coefficients $W_i$, $A_i$, and $Y_i$ for the stiffness matrix and the load vector are given by

$$
\begin{aligned}
W_1 &= 25\rho_2^2 - 4,\\
W_{10} &= 25\rho_{20}^2 - 4,\\
W_2 &= 1 - \rho_2,\\
A_1 &= 75\rho_2^2 - 28,\\
A_2 &= 6875\rho_2^6 + 13125\rho_2^5 - 2725\rho_2^4\\
&\quad - 1800\rho_2^3 - 232\rho_2^2 + 144\rho_2 + 48,\\
A_3 &= 5000\rho_2^7 + 10625\rho_2^6 - 1500\rho_2^5\\
&\quad - 2775\rho_2^4 - 32\rho_2^3 + 72\rho_2^2 + 64\rho_2 + 16,\\
A_4 &= 13\rho_2^2 + 4\rho_2 + 3,\\
A_5 &= 6\rho_2^2 + 2\rho_2 - 1,\\
A_6 &= 2\rho_2^2 + \rho_2 + 2,\\
A_7 &= 2\rho_2^2 + 3\rho_2 + 2,\\
A_8 &= 10\rho_2^5,
\end{aligned}
$$

$$A_9 = 10\rho_2^2,$$
$$A_{10} = 3\rho_2^2 - \rho_2 + 3,$$
$$A_{11} = 5\rho_2^2 + 4\rho_2 + 5,$$
$$A_{12} = 3\rho_2^2 + 4\rho_2 + 13,$$
$$A_{13} = \rho_2^2 - 2\rho_2 - 6,$$
$$A_{14} = 3\rho_2^2 + 9\rho_2 + 23,$$
$$A_{15} = \rho_2^2 + 5\rho_2 + 22,$$
$$Y_1 = 75\rho_2^5 + 175\rho_2^4 + 31\rho_2^3 - 53\rho_2^2 - 12\rho_2 + 4,$$
$$Y_2 = 700\rho_2^4 + 1275\rho_2^3 - 38\rho_2^2 - 18\rho_2 - 8,$$
$$Y_3 = 700\rho_2^4 + 25\rho_2^3 - 138\rho_2^2 + 5\rho_2 - 4,$$
$$Y_4 = 350\rho_2^4 + 650\rho_2^3 + 171\rho_2^2 - 122\rho_2 - 20,$$
$$Y_5 = 350\rho_2^4 + 150\rho_2^3 - 149\rho_2^2 - 208\rho_2 + 4,$$
$$Y_6 = 3\rho_2^2 + 4\rho_2 + 3,$$
$$Y_7 = 15\rho_2^2 - 4,$$
$$Y_8 = 350\rho_2,$$
$$Y_9 = 525\rho_2^4 + 50\rho_2^3 + 11\rho_2^2 - 137\rho_2 - 8,$$
$$Y_{10} = 400\rho_2^3 + 417\rho_2^2 - 340\rho_2 - 36,$$
$$Y_{11} = \rho_2^2 - 2\rho_2 - 9,$$
$$Y_{12} = 175\rho_2^4 + 250\rho_2^3 - 43\rho_2^2 + 218\rho_2 - 12,$$
$$Y_{13} = 175\rho_2^4 - 50\rho_2^3 - 95\rho_2^2 + 284\rho_2 - 20,$$
$$Y_{14} = 175\rho_2^4 + 600\rho_2^3 + 2113\rho_2^2 - 2232\rho_2 - 68.$$

## References


[1] G.L. Hofman, Y.S. Kim, Nucl. Eng. Tech. 37 (2005) 299.
[2] M. Speight, Nucl. Sci. Eng. 37 (1969) 180.
[3] D.R. Olander, Fundamental Aspects of Nuclear Reactor Fuel Elements, Technical Information Center Energy Research and Development Administration, 1976.
[4] K. Forsberg, A.R. Massih, J. Nucl. Mater. 135 (1985) 140.
[5] J.A. Turnbull, J. Nucl. Mater. 50 (1974) 62.
[6] D.M. Dowling, R.J. White, M.O. Tucker, J. Nucl. Mater. 110 (1982) 37.
[7] K. Ito, R. Iwasaki, Y. Iwano, J. Nucl. Sci. Technol. 22 (1985) 129.
[8] J. Rest, J. Nucl. Mater. 321 (2003) 305.
[9] L. Bernard, E. Bonnaud, J. Nucl. Mater. 244 (1997) 75.
[10] J.-S. Cheon, Y.-H. Koo, B.-H. Lee, J.-Y. Oh, D.-S. Sohn, J. Nucl. Mater. 359 (2006) 139.
[11] K. Forsberg, A.R. Massih, J. Nucl. Mater. 127 (1985) 141.
[12] R.J. White, Fission gas release, OECD Halden Reactor Project HWR-632, 2000.
[13] R.J. White, in: ANS International Topical Meeting on Light Water Reactor Fuel Performance, West Palm Beach, Florida, USA, 1994.
[14] A.H. Booth, A method of calculating fission gas diffusion from $UO_2$ fuel and its application to the X-2-f loop test, CRDC-721, 1957.
[15] J. Turnbull, P.V. Uffelen, S. Beguin, The influence of fuel-to-clad gap and $UO_2$ grain size on fission gas release in high burn-up PWR design fuel rods; IFA-519.9, HWR-548, 1998.
[16] ABAQUS, ABAQUS Analysis User's Manual, Version 6.5, 2004.
[17] J.R. Matthews, M.H. Wood, Nucl. Eng. Des. 56 (1980) 439.
[18] K. Lassmann, H. Benk, J. Nucl. Mater. 280 (2000) 127.
[19] C.S. Rim, Background and derivation of ANS-5.4 standard fission product release model, NUREG/CR-2507, 1982.